Alloying Elements and Mechanical Characteristics of Mg-Based Materials

Subjects: Materials Science, Composites

Contributor: Sachin Kumar Sharma , Kuldeep Kumar Saxena , Vinayak Malik , Kahtan A. Mohammed , Chander Prakash , Dharam Buddhi , Saurav Dixit

Magnesium alloys are widely employed in various applications due to their high strength-to-weight ratio and superior mechanical properties as compared to unalloyed Magnesium. Alloying is considered an important way to enhance the strength of the metal matrix composite but it significantly influences the damping property of pure magnesium, while controlling the rate of corrosion for Mg-based material remains critical in the biological environment. Therefore, it is essential to reinforce the magnesium alloy with a suitable alloying element that improves the mechanical characteristics and resistance to corrosion of Mg-based material. Biocompatibility, biodegradability, lower stress shielding effect, bio-activeness, and non-toxicity are the important parameters for biomedical applications other than mechanical and corrosion properties. The development of various surface modifications is also considered a suitable approach to control the degradation rate of Mg-based materials, making lightweight Mg-based materials highly suitable for biomedical implants.

alloying elements corrosion properties surface modifications biocompatibility EW42

1. Introduction

Biomaterials include ceramics, polymers, metallic materials, and composites. In comparison to conventional metals, the biomaterials must have good tensile strength, and ductility, and be able to absorb the strain energy [1]. With these characteristics, orthopedic fixation devices and load-bearing applications including joint replacements, bone plates, screws, rods, wires, cardiovascular stents, and dental implants may be satisfied [2][3]. Traditional metals with strong biocompatibility, such as titanium, cobalt–chromium alloys, and stainless steel are employed as orthopedic implants in fracture treatment [3]. The drawback of these traditional metals was that they were not biodegradable; as a result, in the majority of cases, a second surgery is required to remove the implants from the body after the tissue has healed. Implants typically remain in the body even after the fracture tissue has healed, which increases the risk of infection by allowing the implant material to corrode in a physiological environment [4]. The development of biodegradable implant materials with outstanding corrosion resistance to adapt to the physiological environment is regarded as the current research trend [5][6][7]. Materials that degrade naturally in vivo and in vitro are considered biodegradable. These materials totally disintegrate under the biological state, fulfilling the goal of assisting tissue healing without implant remains [2]. Through the process of dissolution, a non-toxic oxide is created, which is then harmlessly expelled through the urine. Because of this, the primary constituents of

biodegradable materials are those metallic elements that are indigestible to humans and degrade at appropriate rates there.

The three types of biodegradable materials are pure metals, alloys, and metal matrix composites (MMCs) [6]. By selecting the appropriate reinforcement, metal matrix composites, which are biodegradable materials, can display characteristics including yield strength, tensile strength, and young's modulus, as well as corrosion resistance [8]. All components in biodegradable composites should be safe for human health and biodegradable. Magnesium, which is 33% lighter than aluminum and has a density of 1.74 to 2.0 g/cm^3, is the lightest metal [7]. The density of the magnesium substance (1.84 g/cm^3) is extremely similar to that of bone and it has a good strength-to-weight ratio. Due to their required biodegradation and mechanical characteristics, magnesium (Mg) alloys and their composites have been employed as standard implant materials and are being investigated as prospective alternatives [9]. The rate of degradation is extremely high under physiological conditions; as a result, the mechanical integrity of the implant may deteriorate prior to the full healing of the fractured bone tissue. Additionally, a significant amount of hydrogen gases is released, which postpones the healing of the fractured bone tissue [10]. This significant issue has led to the development of pure magnesium, magnesium alloys, and magnesium composites for use in biological applications.

The creation of degradable biomaterial based on magnesium (Mg) has recently attracted more attention. Although Mg is susceptible to corrosion, other physical characteristics, like its low density and high biocompatibility, have spurred major research and development in this field [10]. Several strategies have been used to overcome the problems of corrosion and the poor yield strength of pure magnesium, including the development of composites with suitable bioactive reinforcements, alloying, or surface modifications [10]. In order to maintain the mechanical properties of magnesium alloys and increase their surface biocompatibility for orthopedic applications, surface modification is primarily utilized to regulate the rate of degradation of magnesium alloys. **Table 1** highlights the various surface modification approaches that were incorporated in Mg-based material composites.

Table 1. Surface Modification approaches related to Mg-based materials.

S.NO	Types of Surface Modification Approach	Modification Technique	Description	References
1	Chemical Modification	Acid Etching	1. Removing the initial oxide layer and adding homogenous, and compact layers afterward that slowed the rate of degradation. 2. The impact of acid etching as a pretreatment on the rate of degradation of the magnesium alloy AZ31 in SBF solutions analyzed by Munro et al. 3. In comparison to unetched alloys, homogenous and dense films of $Mg_3(PO_4)_2$ layers were created on etched magnesium alloys, which significantly reduced the rate of degradation.	[11]

S.NO	Types of Surface Modification Approach	Modification Technique	Description	References
2	Chemical Modification	Alkali Treatment	1. After being submerged in an alkaline solution, a new passive layer made up of $MgCO_3$, $Mg(OH)_2$, and MgO is deposited on the surface of magnesium alloys that improving the corrosion resistance. 2. Gu et al. analyzed the reduction in the degradation rate of Mg-based materials in SBF.	[12]
3	Chemical Modification	Fluoride Treatment	1. The most effective and practical method for surface modification of magnesium alloys at the moment is fluorination. 2. In order to create samples of HF-coated magnesium alloys, Li et al. created screws and tensile specimens using magnesium alloys as substrates. Even after a month of immersion, MgF_2-coated samples maintained good mechanical characteristics due to a reduced rate of corrosion than bare samples.	[13]
4	Physical Modification	Sol-gel Coating	1. For a variety of metal substrates, including aluminum, steel, copper, magnesium, and their alloys, sol–gel coatings have been shown to have great chemical stability, excellent oxidation control, and increased corrosion resistance. 2. To reduce the degree of degradation of magnesium alloys, Gaur et al. created a sol–gel silane coating using a combination of diethyl phosphate ethyl tri-ethoxy silane (DEPETES) and bis- [3- (tri-ethoxy silyl) propyl] tetra-sulfide (BTESPT). 3. The samples with the sol–gel coating showed the greatest improvement in the rate of degradation.	[14]
5	Physical Modification	Organosilane coatings	1. For orthopedic purposes, it acts as a protective and biocompatible coating on Mg alloys. 2. The hydrophobic Si-O-Si networks of organosilanes, minor galvanic reactions with Mg, increased adhesive strength, ease of chemical modification, and low cytotoxicity are only a few benefits of employing organosilanes as protective barrier coatings.	[14]
6	Physical Modification	Calcium Phosphate Coating	1. Different procedures have been used to deposit different forms of calcium phosphate coatings, such as hydroxyapatite (HA), fluorinated hydroxyapatite (FHA), and brushite on Mg substrates.	[15]

S.NO	Types of Surface Modification Approach	Modification Technique	Description	References
			2. One of the most effective methods discovered for covering the surface of orthopedic implants is calcium phosphate deposition. 3. The corrosion resistance of Mg alloys covered with Ca-P was greatly increased compared to untreated magnesium alloys, according to Cao et al. who created a Ca-P coating on AZ31 alloys in SBF. Additionally, there were no harmful effects of the Ca-P coating on cells.	
7	Physical Modification	Superhydrophobic Coating	1. One of the most current techniques to increase the corrosion resistance of Mg alloys is a superhydrophobic surface. 2. A superhydrophobic surface with a 157.6° contact angle with water was created by Zhang et al. using AZ31 magnesium alloy. The superhydrophobic coatings considerably increased the corrosion resistance of the AZ31 alloy, according to the corrosion results. 3. Superhydrophobic surfaces inhibit the contact between cells and implants, which limits the implant's capacity to stimulate bone repair and slows the rapid deterioration of magnesium alloys.	[15]

In biomedical applications proposed for the development of orthopedic implants (joint and hip replacement, prosthesis, etc.) and temporary implants, the use of metallic metals has dramatically increased (wires, plates, rods, pins, screws, etc.) [16]. Magnesium has been utilized for more than a century as a biodegradable implant material in vivo and in vitro. Comparing magnesium composites to other metallic metal composites, they had high biocompatibility. Magnesium is a vital component of human life and is the fourth-most prevalent element in the human body [16][17]. **Table 2** compares the value of Mg composites versus Co-Cr alloy, titanium alloys, and stainless steel as implant materials. [18]. It was suggested that the commercially available AZ91D magnesium alloy be used as a matrix in magnesium composites for orthopedic applications after the metallic reaction of the alloy was studied in vivo and in vitro. Magnesium material corrodes quickly and emits hydrogen (H_2) gas, which was observed in a few experiments. Modern techniques were created to slow the pace of corrosion of Mg-based material and cure tissue damage without requiring additional surgery to remove the implanted material [15]. The majority of researchers are working to produce implants for orthopedic applications and cardiovascular stents using biodegradable Mg-based materials [12][13][14][15][16]. **Table 3** identified the mechanical properties of Mg alloy and other metallic implant materials.

Table 2. Comparison of Mg alloy with other metallic implants.

S.NO	Material	Benefits	Drawbacks	Applications
1	Co-Cr alloy	1. Provides good resistance to fatigue, wear, and corrosion.	1. Very expensive. 2. Machining is difficult.	1. Bone implantation (wires and plates). 2. Hip replacement.

S.NO	Material	Benefits	Drawbacks	Applications
		2. Provides high strength. 3. Long-span biocompatibility.		
2	Ti alloy	1. Enables good corrosion resistance and has low young's modulus with suitable biocompatibility. 2. High strength than 316L stainless steel.	1. High wear rate. 2. Very expensive.	1. Fracture fixation. 2. Total joint replacement.
3	316L Stainless steel	1. Easily available, high toughness, suitable biocompatibility, inexpensive, and good fabrication characteristics.	1. High corrosion, and wear rate, high-stress shielding effect.	1. Bone implantation.
4	Mg-alloy	1. Biocompatible, bioresorbable, biodegradable, and bio-active. 2. Elastic modulus resembling human bone. 3. Low-stress shielding effect and lightweight.	1. High H_2 evolution during degradation	1. Bone implantation, screws, and plates.

S.NO	Material Property	Human Bone	Mg Alloys	Ti Alloys	Co-Cr Alloys	Stainless Steels
1	Density (g/cm^3)	1.8–2.1	1.74–2.00	4.4–4.5	8.3–9.2	7.9–8.1
2	Yield Strength (MPa)	30–114.3	20–200	896–1034	448–1606	221–1213
3	Compressive Strength (MPa)	164–240	55–130	N/A	N/A	N/A
4	Young's Modulus (GPa)	3–23	41–45	110–117	210–232	189–205
5	Fracture toughness (MPa/m$^{1/2}$)	3–7	15–40	55–115	50–200	NA
6	Tensile Strength (MPa)	70–150	86–280	760–1140	655–1896	586–1351
7	Elongation (%)	1.07–2.10	12–21	12	N/A	N/A

It has been suggested that graphene is a wonder material with great charge carrier mobility, large surface area, and exceptional mechanical characteristics. Additionally, graphene's long-extend π-conjugation is a crucial photocatalytic characteristic that enables a variety of biosensor activities. Due to the broad application of nanographene, recent developments in biomedical applications and materials science, such as scaffold, cancer nanotechnology, tissue manufacturing, drug delivery, and antimicrobial activities, have been incorporated [17]. Graphene-assembly nano biosensors are now one of the top choices among researchers since they are safe to use, cost-effective, less time-consuming, and most importantly used for the daily assessment of glucose levels [18]. The use of nanoparticles (NP) to eradicate bacteria that are free-floating and those that form biofilms is one of their

important applications in healthcare [19]. It has been demonstrated that a number of nanoparticles, including CuO, Fe_3O_4, ZnO, MgO, Al_2O_3, etc. can accomplish this property with varying levels of functionality. Using nanocomposite (NC) materials to remove germs is a more sophisticated and effective technique to destroy bacterial biofilms. Materials similar to chitosan and graphene can also be utilized to make several forms of the nanocomposite, in addition to different metal oxides [20]. The capacity of nanoparticles and nanocomposites to avoid the issue of bacterial resistance is one of their main advantages over antibiotics. In biomedical applications such as hip joints, cardiovascular stents, bone fixation, and dental implants, the Mg-based bio-composite is used [20].

Biodegradable metals (BMs) slowly deteriorate in living tissue by generating corrosion products when they are in contact with the body's physiological conditions [21]. Biodegradable implants that completely dissolve with no implant material left in the surrounding tissues help in the recovery and repairing of tissue bone. Three kinds of BMs—Fe-based, Mg-based, and Zn-based BMs—have undergone substantial research in recent years. Mg-based materials have undergone the most clinical testing among the three BMs. While Fe-based BMs show slower and less complete in vivo breakdown, Mg-based BMs often exhibit higher degradation rates, which might not match the bone tissue's healing times. Due to their intermediate degradation rates, which fall between those of Mg-and Fe-based BMs, Zn-based BMs are now regarded as a new class of BMs [22]. Hussein et al. analyzed the corrosion behavior of eggshell-reinforced Mg and Mg-Zr alloy and observed that the eggshell has the potential to be exploited as efficient green reinforcing particles in the creation of Mg and Mg-Zr-based composites, with better in vitro corrosion characteristics for biomedical applications [23].

By advancing green chemistry to create "Greenery Nanoscience and Nanotechnology," nanoscience ensures a promising future. The "Green Chemistry" technique, which is attributed to the bigger pore volume and long-range surface area of gold nanoparticles, is the one and only outstanding method authenticated for the enhancement and execution of chemically assisted processes in order to limit the usage of toxic compounds [24]. Currently, low-cost natural and waste products have been treated with hazardous chemicals to produce value-added nanomaterials with wide applications, proposing an affordable and environmentally friendly solution to environmental problems.

Magnesium-based alloys had received a lot of attention as potential biodegradable implant materials in biomedical applications [1][2][3]. For orthopedic applications, a new generation of bioactive, biocompatible, and biodegradable metallic materials has recently been discovered. Due to its great biocompatibility and adequate strength, pure magnesium, magnesium alloys, and magnesium alloy-based composites are widely used in biomedical applications [25]. In a biological environment, pure magnesium and magnesium alloys can corrode too quickly and lose their characteristics before bone healing. The new era of composites made of magnesium can meet the needs of orthopedic applications. Magnesium-based composites are biomaterials that can create suitable mechanical properties under a biological environment, such as ultimate tensile strength, elastic modulus, ductility, and resistance to corrosion [26]. The matrix materials used in magnesium-based composites, such as Mg-Zn, Mg-Al, Mg-Ca, and Mg-REE alloy, are biomedical magnesium alloys [27]. The usage of Mg alloys as biomaterials enriches the growth of magnesium alloys in biodegradable metallic implants that showcase the influence of alloying elements such as Al, Zn, Li, Mn, Zr, Ca, Sr, and rare earth elements on resistance to corrosion, mechanical

characteristics, and biocompatibility of Magnesium alloys. Ce, Gd, yttrium, lanthanum, erbium, and neodymium are the somewhat-rare earth elements employed as an alloying element in Mg alloys [3].

2. Classification of Mg Alloy and Influence of Alloying Element on Various Mg Alloys

The alloying element such as aluminum, titanium, and magnesium are widely used in technologies and are the most suitable substitute for steel employed in structural applications [3]. Mg alloys have the lightest structure of all the non-ferrous element metals [5]. Therefore, one research study suggested that the usage of Mg-based alloys has increased in biomedical and structural applications [6]. During the formation of Mg-based alloys in biomedical applications, biocompatibility is the most important factor that governed the effectiveness of bone-implant and tissue regeneration without any toxic effects on living tissues [28]. The Mg-based alloys can be classified as wrought and cast magnesium alloys based on the processing approaches required for engineering applications and research and development perspectives [29]. The Mg alloys obtained via die and various casting approaches are referred to as-cast alloys [30]. The research study suggested that cast Mg alloys can be employed in limited areas where reasonable mechanical properties are required and are commonly used in industrial and commercial applications [6]. The wrought Mg alloys are obtained via secondary manufacturing processes such as Rolling, Equal-Channel Angular Pressing (ECAP), Extrusion, and Severe Plastic Deformation (SPD), while SPD is the most suitable approach for a reduction in grain size in microstructure characterization [31]. The researcher's approach suggested that the wrought Mg alloys had remarkable mechanical properties as compared to cast Mg alloys [30]. The wrought alloys enable the homogenous composition of alloy along with grain refinement having no pores on the surface of the alloy [29]. The classification of various magnesium alloys was illustrated in **Figure 1**. The Mg alloy can be binary, ternary, and quaternary subject to the presence of several phases and alloying elements in the alloy [32].

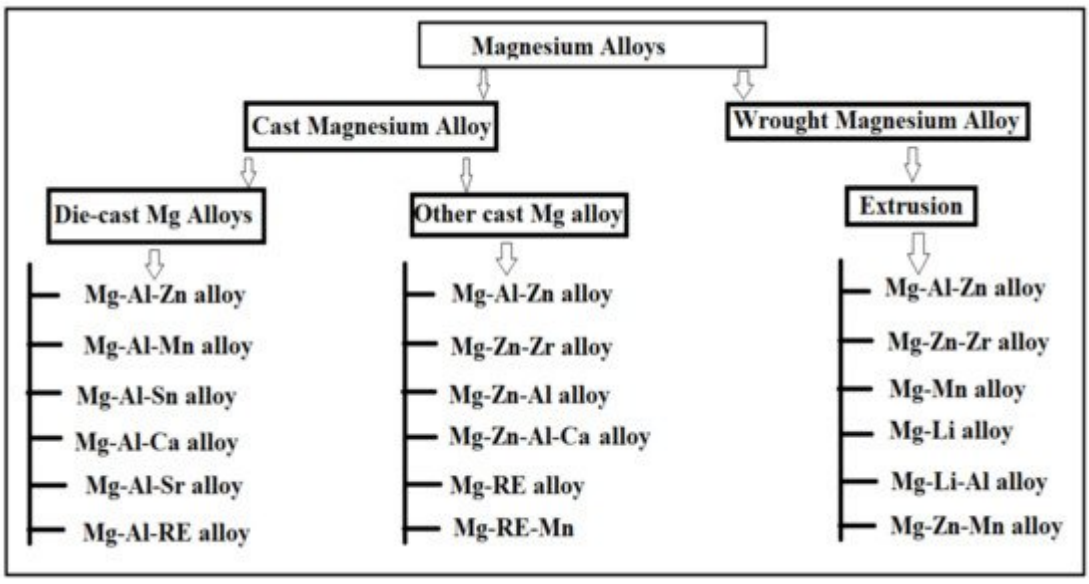

Figure 1. Classification of various Mg-based alloys.

2.1. Mg-Al Based Alloys

When aluminum is dissolved in Mg, the formation of the α-Mg phase and ϒ-$Mg_{17}Al_{12}$ phases (eutectic ternary phases) occur which enhances the solid-solution strength [33]. Mg-Al alloy is the most predominantly used Mg alloy due to its high specific stiffness, high specific strength, good electromagnetic shielding, good vibration properties, good anti-radiation properties, and other characteristics. Thus, Mg-Al alloys, also referred to as the “green engineering materials of the twenty-first century,” have a wide range of potential applications in automobiles, electrical equipment, electronics, transportation, aviators, and biomedical application fields [33]. Mg-Al alloys are vitally used in bone implantation with good tissue healing and low-stress shielding effect on the implant. The literature suggests that the mechanical properties (compressive and tensile strength) of Mg-Al binary alloys with Al content that exceeded the solubility limit significantly increased. Furthermore, the addition of more than 6 wt.% of Ca in the Mg-Al alloy significantly improves the tensile and compressive strength of the Mg-Al alloy. The Mg–Al-based alloys have superior castability with average mechanical properties [34]. The most commonly used alloying element in Mg-Al alloys is zinc and manganese with a concentration of around 1 wt.% [33]. The Mg-Al-based alloys usually have AM, AE, and AZ series which are biodegradable in nature that involves AM60, AZ31, AZ81, AZ61, and AZ91 alloys [34]. The AZ31 alloy indicates A as aluminum and Z as zinc and number 3 and 1 indicate 3% of Aluminum and 1% of zinc, respectively [28]. The AM series comprises various alloys involving Mg inclusive of aluminum and manganese such as AM30, AM40, AM50, and AM60, etc. [35]. The AM-based alloy has higher mechanical properties and suitable extrudability in comparison with AZ alloys having an absence of eutectic ternary phases containing zinc [33]. The Mg-based alloys involve the addition of zinc to provide strength to solute particles, but Manganese is added to improve the anti-corrosion properties of the alloy by eliminating the patches of iron from the alloy [36]. The Mg-Al-based alloys have negligible age-hardening due to the formation of the β-$Mg_{17}Al_{12}$ phase [33]. About 70% of the grains identified in microstructures are recrystallized to an average grain size of 1.2 μm [34][35][36][37]. The various Mg-Al alloys along with the effect of the alloying element are illustrated in the below section.

2.1.1. AZ Alloy Series

The addition of alloying element lithium in AZ31 alloy has optimized the microstructure of the alloy, as lithium enables the formation of a cross and non-basal slip [38]. Lithium is highly soluble in AZ31 alloy, allowing the alteration in lattice parameters of a solid solution of magnesium [38]. For an increase in the amount of lithium in AZ31 alloy, the random distribution of grains around the boundaries and a large reduction in basal structure intensity are obtained [39]. Additionally, lithium also promotes an enhancement in ductility and reduction in anisotropy of AZ31 alloy due to the recrystallization of grains around the boundary [38]. The tensile strength of the alloy remains the same with the addition of lithium [39]. The research study by Meng et al. suggested that a high value of elongation and tensile strength were found in Mg-1Al-1Zn-8Li, these being 9.2% and 233.38 MPa, respectively [40][41]. The addition of tin in Mg-Al alloy enhanced the compressive and tensile properties of Mg-Al-based alloy composite due to a reduction in the stacking energy in the alloy [42]. Wu et al. suggested that the grain size in AZ91 is refined via the addition of tin in hot extrusion due to the restriction in the formation of Mg_2Sn precipitates around the grain boundary [43]. The rare earth elements in Mg-Al alloys allow the formation of thermally stable phase $(Mg, Al)_xRE_y$ as a result of that the enhancement in the mechanical properties of wrought Mg alloys

that occurs [43]. The microstructure of the alloy AE44 (Mg-4.0Al-4.1RE-0.3Mn, wt.%) produced here mostly consists of α-Mg grains and $Al_{11}RE_3$ intermetallic phase at grain boundaries. Additionally, TEM images depict a lamellar phase with primarily $Al_{11}Ce_3$ indicated in **Figure 2** [44]. The TEM also found trace phases. Both the lamellar phase and the feather-like phase contain La, Ce, Nd, and Al with an Al/RE ratio near 11:3, according to the results of the EDX micro-analysis, and the XRD pattern further demonstrates that the inter-metallics are a part of the $Al_{11}RE_3$ phase ($Al_{11}Ce_3$) [44]. Pan et al. analyzed the effects of yttrium on the microstructure and mechanical properties of AZ31 alloy [45]. At 0.5 wt.% of yttrium in Mg-Al alloy, high yield strength of around 209 MPa was observed due to the formation of the Al_2Y phase [46]. At 0.9 wt.% of yttrium in AZ31, the optimal mechanical properties were obtained, i.e., YS (yield strength), UTS (ultimate tensile strength), and elongation (%) are 258.9 MPa, 371.9 MPa, and 7.33% due to refinement in grain size of the Al_2Y phase [46]. The coarse and brittle Al_2Y phase was obtained at 1.4 wt.% of yttrium in AZ31 which causes a reduction in the tensile strength of the alloy [46].

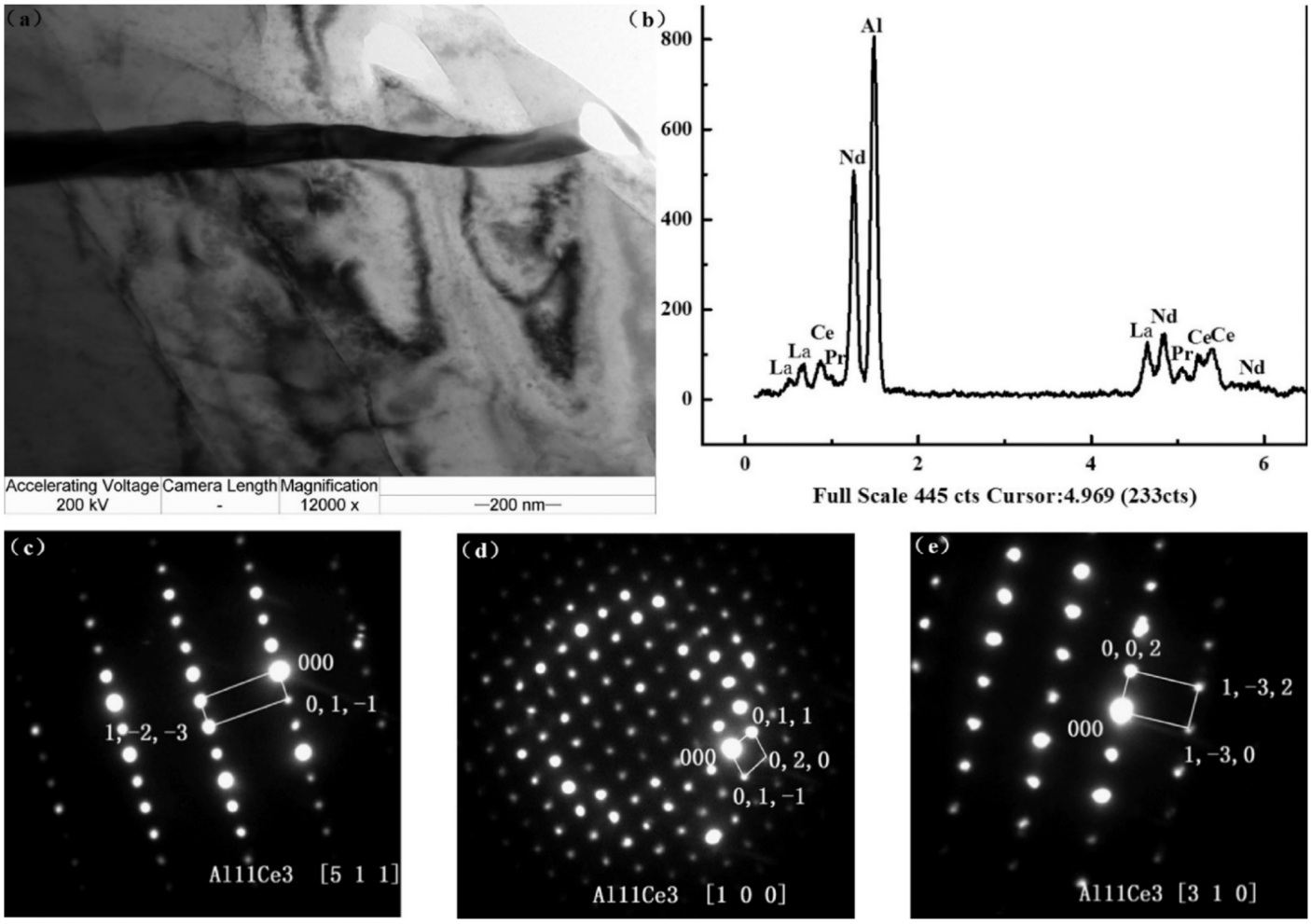

Figure 2. (**a**) TEM bright-field image; (**b**) EDX spectrum; and (**c**–**e**) SAED patterns ([511] zone, [100] zone, [310] zone axis, respectively) of the Al11Ce3 precipitates in unreinforced AE44 alloy [44].

The addition of 0.12 wt.% Mn as an alloying element in the Mg-Al alloy eventually replaces the Al-Fe phase with the Al_8Mn_5 phase. **Figure 3**a illustrates the XRD image of the Mg-3Al-xMn alloy depicting the presence of Al_8Mn_5 and MgF_2 in the alloying composition (Mg-3Al-0.12Mn and Mg-3Al-0.21Mn), respectively. During the

creation of the samples, the MgF_2 phase was produced by the reaction of the Mg melt with the safety of SF_6 gas. The potentiodynamic polarization curve for each sample of Mg-3Al-xMn was analyzed in a 3.5 wt.% of NaCl solution depicted in **Figure 3**b [47]. The cathodic branches of the polarization curves of the alloys with Mn added were smaller than those of the alloy with Mg-3Al, indicating a decrease in the cathodic hydrogen reaction. The anodic polarization curves of the Mg-3Al-0.36Mn and Mg-3Al-0.45Mn alloys showed clear passivation behavior, although the curves of other alloys had active dissolving features. Additionally, the breakdown potential (E_b) of the passive film (depicted by the black arrow) was obtained. The current density steadily reduced as Mn addition increased, and was observed to be the lowest for Mg-3Al-0.45Mn alloy. The higher value of (E_b-E_{corr}) indicated a passivation film that was more stable [47]. The breakdown potential for Mg-3Al-0.45Mn (94 mV) was observed to be higher than the Mg-3Al-0.36Mn alloy, suggesting that the passive film was more stable, indicating the lower propensity to develop localized corrosion. Therefore, corrosion resistance was observed to be enhanced with the addition of Mn to Mg-Al alloy.

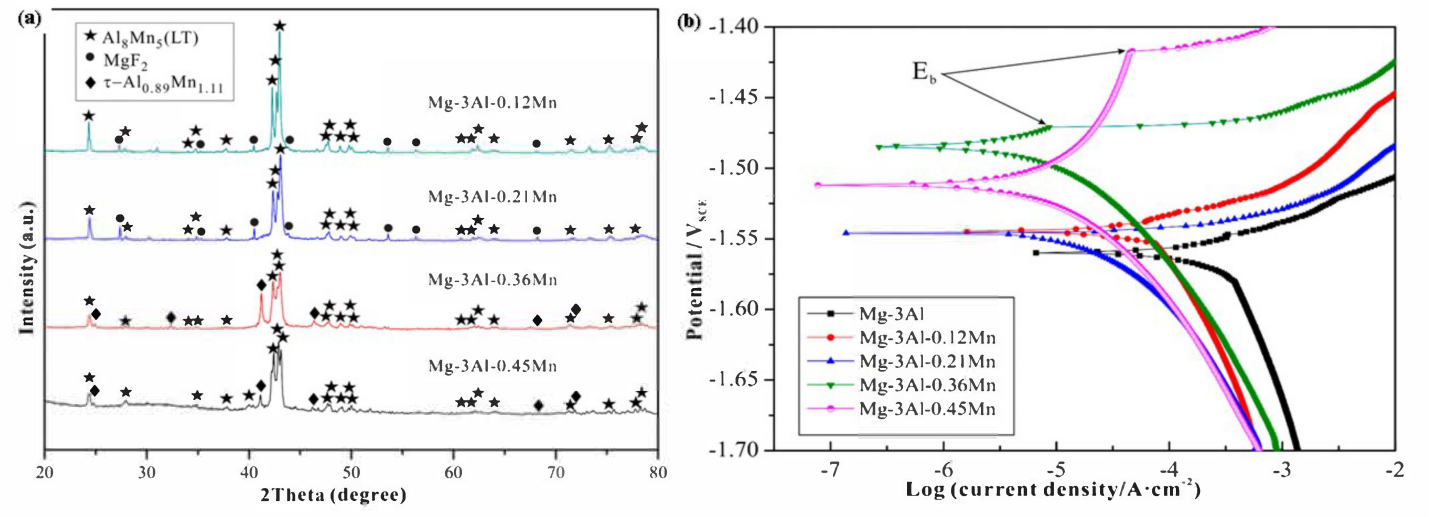

Figure 3. (**a**) XRD image of Mg-3Al-xMn alloys (x = 0.12, 0.21, 0.36, 0.45). (**b**) Polarization curves of the Mg-3Al-xMn alloys (x = 0.12, 0.21, 0.36, 0.45) in 3.5 wt.% NaCl solution, with the arrow indicating the breakdown potential (E_b) [47].

The addition of alloying element, calcium enhances the strength of Mg-Al-based alloys due to the presence of a stable Al_2Ca phase in Mg-Al alloy [12]. For around 1.7 wt.% of calcium in Mg-2.32Al alloy, the refinement in grain occurs around the boundary which leads to an increase in UTS (ultimate tensile strength), elongation (%), and YS (yield strength) to about 324 MPa, 10.2%, and 275 MPa respectively [48]. The FE-SEM imaging shows that the broken Al_2Ca phase is present which leads to improvements in the mechanical properties of the alloy. The comparative study of AZ31 alloy both with and without calcium shows that calcium in AZ31 provides better mechanical properties with finer grains and high ductility [11]. Kwak et al. concluded that calcium in AZ31 leads to a refinement in grain size and obtained a uniform composition of the alloy at 0.5 wt.% of calcium [40]. The alloys Mg-3.2Al-3.3Ca-0.7Mn (AX33), Mg-4.2Al-4.3Ca-0.7Mn (AX44), and Mg-5.1Al-5.2Ca-0.7Mn alloy (AX55) were created to highlight the relationship between microstructure and characteristics of Mg alloys with high Ca/Al ratios. XRD images of all three alloys depicted the α-Mg solid solution and Al_2Ca phase depicted in **Figure 4**A. It was further

concluded that when the ratio of Ca/Al was less than 0.8., then the Al_2Ca phase formed but (Mg, Al)$_2$Ca or (Mg, Al)$_2$Ca + Mg_2Ca phases were produced when the Ca/Al ratio was more than 0.8 [49]. **Figure 4**B depicted the OM image of the as-cast ingots of AX33, AX44, and AX55, indicating that the as-cast ingots had the presence of reticular (Mg, Al)$_2$Ca + α-Mg solid solution. The grain boundary of the α-Mg solid solution was dispersed with the reticular (Mg, Al)$_2$Ca phase. As the amount of Ca and Al in the as-cast ingots increased, so did the volume percentage of the (Mg, Al)$_2$Ca phase [49].

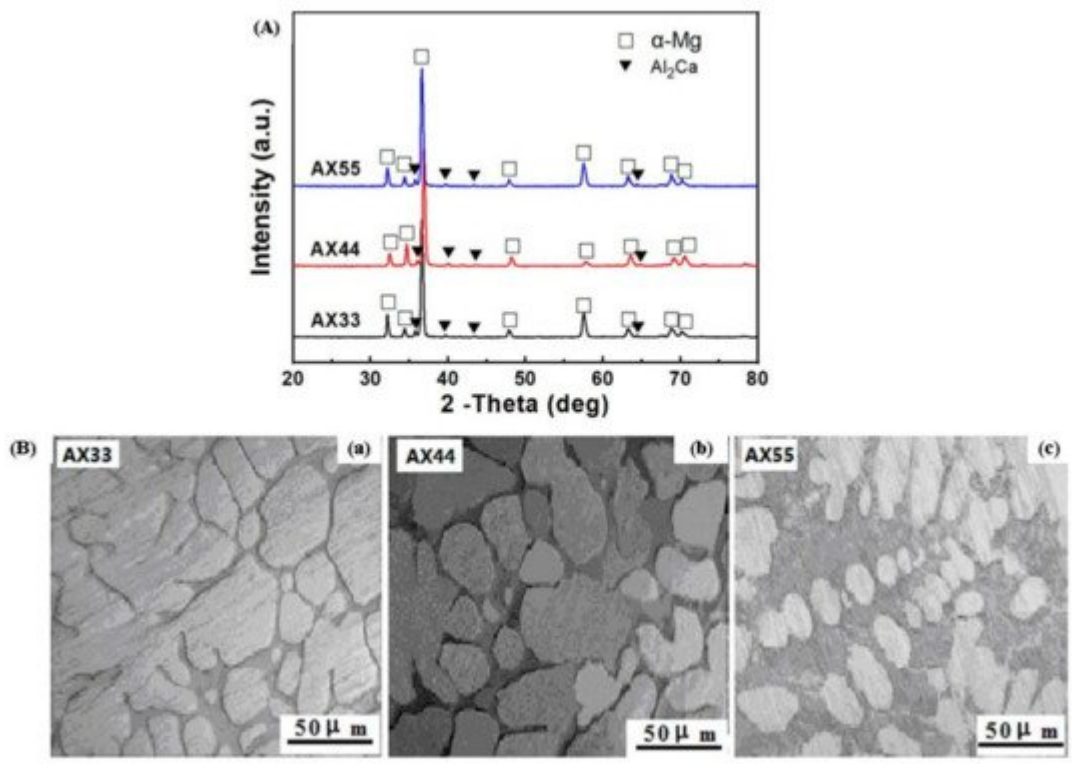

Figure 4. (**A**) XRD image of the as-extruded AX33, AX44, and AX55 alloys. (**B**) Optical microscopy of the as-cast ingots of (**a**) AX33, (**b**) AX44, and (**c**) AX55 alloy [49].

The alloying element strontium in Mg-Al-based alloy enhances the mechanical properties of the alloy due to the presence of a stable Al_4Sr compound [48]. The addition of 0.02 wt.% of strontium to double-hot-extruded Z80 alloy enhances the elongation (%) and UTS (ultimate tensile strength) to 13.2% and 355 MPa, respectively [50]. However, one research study suggested strontium decreases the solubility of aluminum in Mg alloys, as it hinders the formation of the β-$Mg_{17}Al_{12}$ phase, which has an adverse effect on mechanical properties [42]. The increase in the amount of tin in AZ91 restricted the formation of the discontinuous β-$Mg_{17}Al_{12}$ phase, but up to 4 to 5 wt.% of tin promotes reduction in the discontinuous β-$Mg_{17}Al_{12}$ phase and improved the mechanical property as compared to AZ91 alloys, as the density of fine precipitates is continuously increasing [48]. The electromagnetic stirring of AZ91 alloy refines the α-Mg and β-$Mg_{17}Al_{12}$ grains (due to the rise in nucleation rate), and creates a few tensile twins, increasing the ultimate tensile strength, yield strength, and elongation to 187mpa, 167mpa, and 7.5%, respectively. Electromagnetic stirring increases the ductility of the AZ91 alloy, which has low plasticity and enhances the application field of AZ91 alloy [51]. XRD imaging of AZ91 alloy depicted the α-Mg and β-$Mg_{17}Al_{12}$ phase, but after electromagnetic stirring, there is only the α-Mg matrix peak visible, reducing the volume

of β-$Mg_{17}Al_{12}$. **Figure 5**A depicted the SEM image of AZ91 alloys, indicating the Mg matrix and white secondary phases (β-$Mg_{17}Al_{12}$). The unmodified sample involves the α-Mg matrix, β-$Mg_{17}Al_{12}$ phase and eutectic α + β phases. The eutectic α + β phase (lamellar) and β-$Mg_{17}Al_{12}$ phase (coarse dendrites) are mainly distributed on the grain boundary. The modified sample of AZ91 alloy indicates the partial breaking of the eutectic α+β phase and the reduction of the β-$Mg_{17}Al_{12}$ phase resembling the more uniform dispersion of β-$Mg_{17}Al_{12}$ phase induced by electromagnetic stirring [51]. EBSD mapping of AZ91 alloy shown in **Figure 5**B indicated low-angle grain boundaries (LAGBs) with misorientation within 2°–10°, which are designated by a white line, while high-angle grain boundaries (HAGBs) with misorientation larger than 10° are indicated by a black line. The microstructure of the unmodified specimen showed that the fraction of grains with a significant misorientation angle of 15°–90° is more uniform and that the proportion of grains with a misorientation angle less than 5° is relatively high [51]. The grains of the modified specimen contain a significant number of grains with LAGBs and fractured substructures together with a small number of {1012} tensile twins. Because of the occurrence of twinning inside the AZ91 alloy during the electromagnetic stirring, the HAGBs are primarily dispersed between 80° and 90°, and the misorientation angle distribution of 85°–90° existed in the sample. The TEM image of the AZ91 alloy is shown in **Figure 5**C indicating that the unmodified AZ91 alloy depicted some spherical particles ($Mg_{17}Al_{12}$ phase) and a modified sample refined and uniformly distributed the $Mg_{17}Al_{12}$ phase in the AZ91 alloy [51].

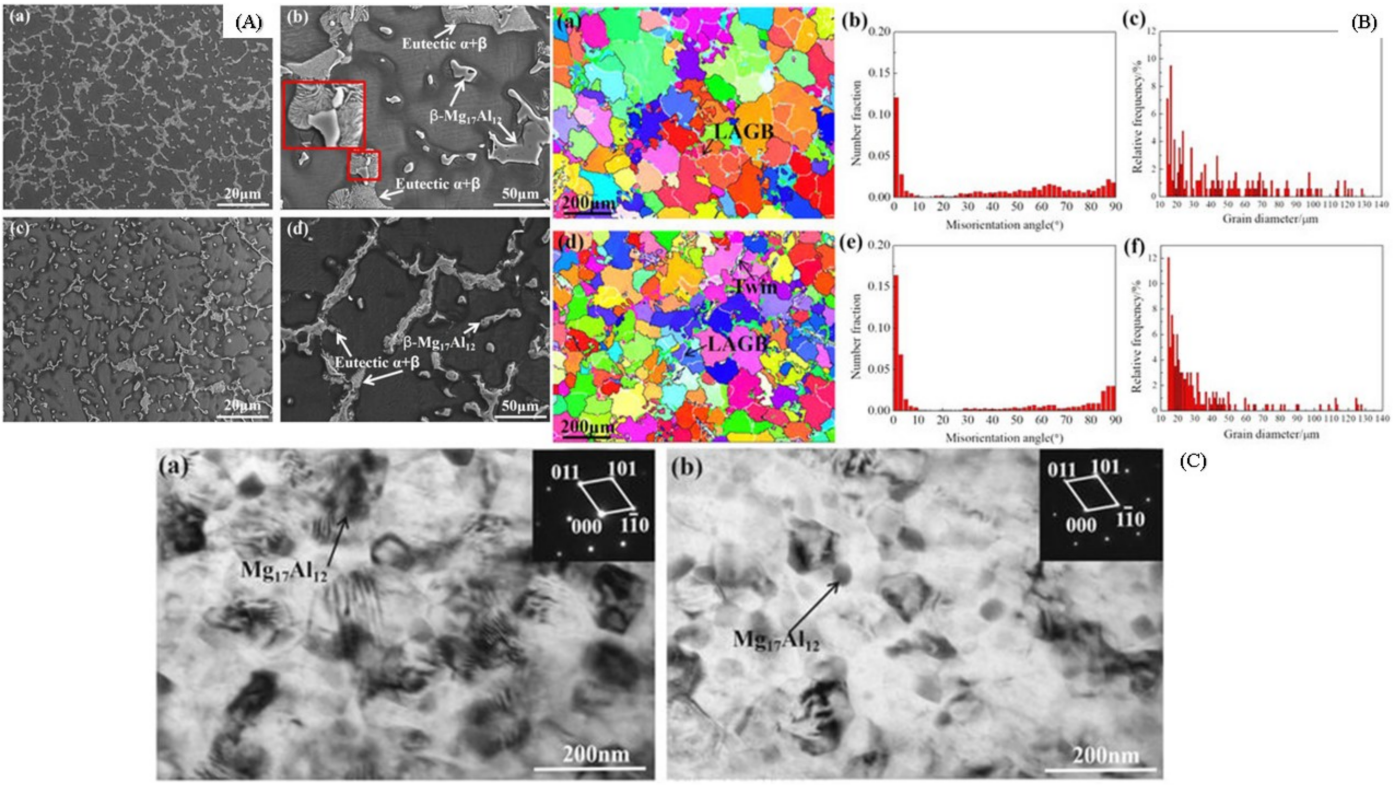

Figure 5. (**A**) SEM image of AZ91 alloy (**a**,**b**) unmodified sample, (**c**,**d**) modified sample. (**B**) For unmodified AZ31 alloy (**a**) EBSD mapping (**b**) Misorientation angle, and (**c**) Grain diameter distribution; For modified AZ31 alloy (**d**) EBSD mapping, (**e**) Misorientation angle, and (**f**) Grain diameter distribution. (**C**) Bright-field TEM image of AZ91 alloy (**a**) Unmodified, and (**b**) Modified sample [51].

2.2. Mg-Zn Based Alloys

Zinc is considered one of the most commonly used alloying elements other than aluminum, which improves the mechanical properties of magnesium-based material alloys [52]. Compared with aluminum, zinc is regarded as a biocompatible alloying element alongside being seen as an important element present in the body, fulfilling nutrient availability. Therefore, it is regarded as the most suitable alloying element used in biomedical applications [53]. The main components/phases depicted in Mg-Zn alloy are α-Mg and ϒ-MgZn phases [54]. The solubility of zinc in magnesium is found to be highest at around 6.2 wt.% but drops sharply to about 2.6 wt.% [48]. The increase in the concentration of zinc content increases the YS (yield strength) of the Mg-Zn alloy and the ultimate tensile strength (216.8 MPa) and elongation (15.8%) and obtained to be maximum of around 4 wt.% of zinc [55]. Adding alloying elements such as zirconium, calcium, silicon, yttrium, strontium, and manganese provides a significant improvement in the mechanical properties of magnesium–zinc-based alloys [8]. **Figure 6**a indicates the optical energy band gap (E_g) of $Mg_xZn_{1-x}O$ thin films (function of Mg^{2+} concentration), and **Figure 6**b showed the tabulated data representing the optical band gap, RMS, and grain size for AFM image of $Mg_xZn_{1-x}O$ thin film [56]. The successive ionic layer adsorption and reaction (SILAR) approach was used to generate a sequence of $Mg_xZn_{1-x}O$ thin films on glass substrates. It has been noted that the deposited films are polycrystalline in nature and have grown in hexagonal and cubic phases [56]. The film preferred orientation was absorbed along the {002} plane. As the Mg^{2+} ions content rises, the crystallite size and surface roughness also do. The outcomes thus demonstrated that the Mg^{2+} ions content can regulate the surface topography and surface quality of the deposited films [56]. The optical transmittance spectra investigation revealed that the energy band gap increased (2.82–3.17 eV) as the Mg^{2+} concentration increased for x = (0.25–0.75), and the transmittance increased with the rise of Mg^{2+} content to around 85% [56]. These findings suggest that high-performance ultraviolet optoelectronic devices may be made using $Mg_xZn_{1-x}O$ thin films. The various alloying elements employed in the Mg-Zn alloys are listed below.

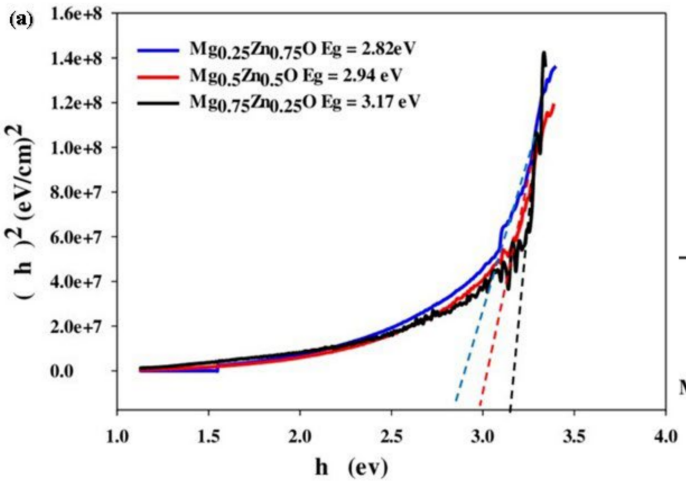

(b)

Compound	Band gap (eV)	Transmittane %	Roughness Average nm	Root mean square nm	Grain diameter AFM
$Mg_{0.25}Zn_{0.75}O$	2.82	70	20.9	25	89
$Mg_{0.5}Zn_{0.5}O$	2.94	62	31.2	39.1	91
Mg0.75Zn0.25O	3.17	59	23.8	28.3	100

Figure 6. (**a**) Optical energy band gap (E_g) of $Mg_xZn_{1-x}O$ thin films (function of Mg^{2+} concentration), (**b**) Tabulated data representing the optical band gap, RMS, and grain size for AFM image of $Mg_xZn_{1-x}O$ thin film [56].

2.2.1. Mg-Zn-Ca Alloys

Mg-Zn-Ca alloy is cost-effective and has superior mechanical properties among all Mg-Zn alloys [11]. The presence of calcium in Mg-based alloy acts as a grain refiner [11]. However, the mechanical properties of Mg-Zn-based alloys are reduced when the concentration of calcium increases beyond 1% due to the reduction in the solubility of calcium [10]. The research study suggested that the Mg-1Zn-0.5Ca alloy results in an improvement in mechanical properties of the alloy at hot extrusion due to the refinement in grain size and weakening of base texture via 0.5 wt.% Ca in Mg-Zn alloy [57]. The ultimate tensile strength was observed to be maximum up to 1 wt.% of Ca in Mg-Zn alloy due to the formation of sharp substrate texture, and partial recrystallization of microstructure [57]. The surface morphology of the alloy Mg-4.0-Zn-0.2-Ca indicated by optical microscopy is illustrated in **Figure 7**a,b of the Mg-4.0-Zn-0.2-Ca alloy [58]. The researchers experimentally verified that the extruded Mg-Ca-Zn-Zr alloy was tested with a low concentration of Zn and Ca content, i.e., around 1 wt.%, obtained the elongation (11%) and tensile strength (306 MPa) [48]. The Zener pinning dynamic recrystallization of fine precipitates refines the microstructure of magnesium–calcium-based alloys [59]. The research study analyzed the addition of 0.8 wt.% Zr in Mg-6Zn-0.2Ca alloy (ZX60) showed an improvement in tensile yield strength from 148 MPa to 310 MPa [58]. When manganese, calcium, and zinc are added in a dilute state, it exhibits balanced ductility and yield strength along with an improvement in the extrudability of the alloy subtending to high specific strength that widens the application of Mg-based alloy, making it suitable for broad industrial applications [48].

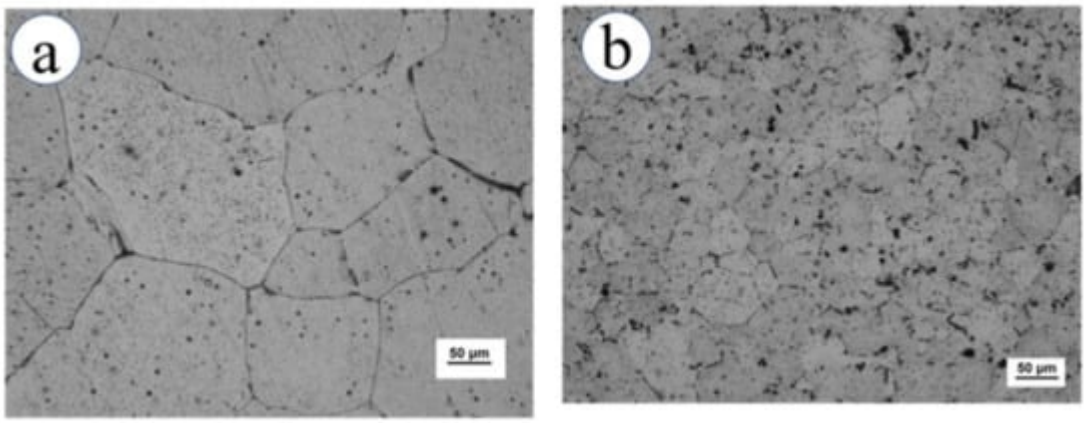

Figure 7. (**a**,**b**) Optical micrograph of Mg-4.0-Zn-0.2-Ca [58].

2.2.2. Mg-Zn-Mn Alloys

Mg-Zn-Mn alloy has high strength, excellent resistance to corrosion, and high ductility [48]. The extruded Mg-5.99Zn-1.76Ca-0.35Mn alloy has superior mechanical properties involving a yield strength of 289MPa and an elongation of 16% [40]. With the addition of 0.3% of Mn in Mg-Zn-Ca alloy, the improvement in yield strength was observed and obtained to be 50MPa, but the addition of about 2 wt.% of Mn to extruded Mg-2Zn alloys, also improved the yield strength and ductility of alloy along with the refinement in grain size and produced the improvement in sliding resistance [60]. The research study suggested that the addition of manganese improves the tensile strength and ductility of pure Mg by around 204.3 MPa and 38.8% respectively [27]. Along with manganese, the addition of silicon to Mg-Zn alloy improves the yield tensile strength of the alloy and is observed to be around

200–240 MPa [60][61][62][63]. A significant density of Al, Mn intermetallic particles can be seen in the matrix in **Figure 8**a,b representing FE-SEM/EDS imaging and AFM imaging of β-$Mg_{17}(Al, Zn)_{12}$ precipitates, α-Mg solid solution, and Al, Mn particles after mechanical polishing [64]. FE-SEM/EDS measurements revealed a composition of 38.1 ± 2.1 (%) Al and 44 ± 5 (%) Mn. These particles have a diameter of 0.5 to 5 µm. The results of the FE-SEM/EDS studies showed that they were composed of Mg (61.3%), Al (64.4%), Zn (3.4%), O (1%), Mn (0.3%), Ni (0.37%), and Cu (0.2%). AFM imaging did not identify any micro-voids at the point where the massive precipitates contacted the metallic matrix [64].

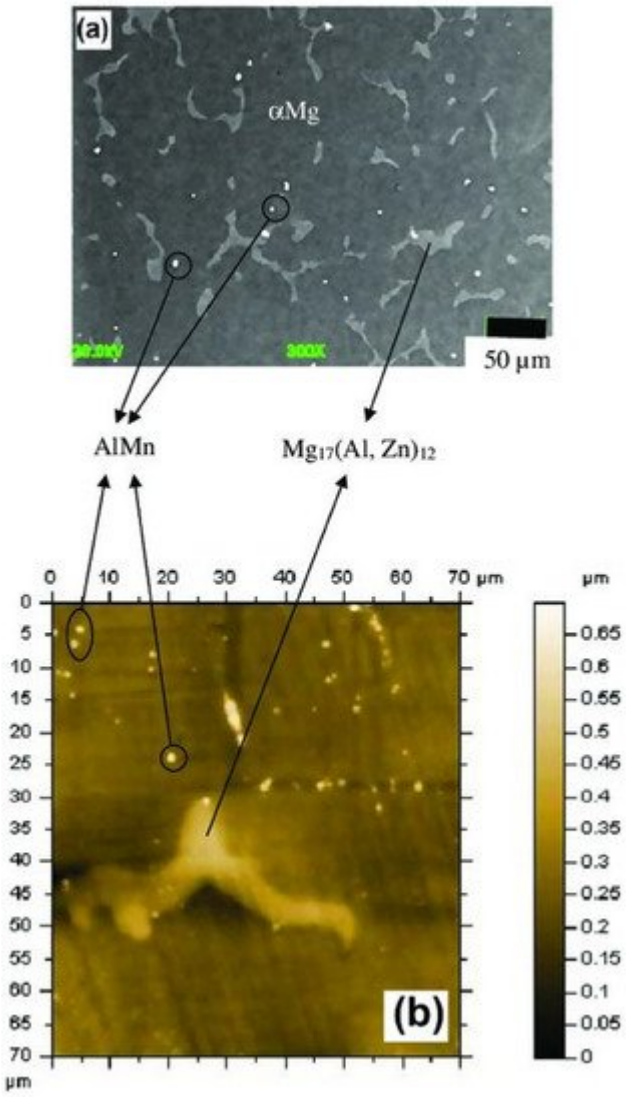

Figure 8. (**a**) FE-SEM/EDS imaging (**b**) AFM imaging of β-$Mg_{17}(Al, Zn)_{12}$ precipitates, α-Mg solid solution, and Al, Mn particles after mechanical polishing [64].

References

1. Singh, H.; Singh, S.; Prakash, C. Current trends in biomaterials and bio-manufacturing. In Biomanufacturing; Springer: Cham, Switzerland, 2019; pp. 1–34.

2. Singh, H.; Prakash, C.; Singh, S. Plasma spray deposition of HA-TiO2 on β-phase Ti-35Nb-7Ta-5Zr alloy for hip stem: Characterization of bio-mechanical properties, wettability, and wear resistance. J. Bionic Eng. 2020, 17, 1029–1044.
3. Prakash, C.; Kansal, H.K.; Pabla, B.S.; Puri, S.; Aggarwal, A. Electric discharge machining–A potential choice for surface modification of metallic implants for orthopedic applications: A review. Proc. Inst. Mech. Eng. Part B J. Eng. Manuf. 2016, 230, 331–353.
4. Prakash, C.; Singh, S.; Gupta, M.K.; Mia, M.; Królczyk, G.; Khanna, N. Synthesis, characterization, corrosion resistance and in-vitro bioactivity behavior of biodegradable Mg–Zn–Mn–(Si–HA) composite for orthopaedic applications. Materials 2018, 11, 1602.
5. Arora, G.S.; Saxena, K.K.; Mohammed, K.A.; Prakash, C.; Dixit, S. Manufacturing Techniques for Mg-Based Metal Matrix Composite with Different Reinforcements. Crystals 2022, 12, 945.
6. Prakash, C.; Singh, S.; Pabla, B.S.; Sidhu, S.S.; Uddin, M.S. Bio-inspired low elastic biodegradable Mg-Zn-Mn-Si-HA alloy fabricated by spark plasma sintering. Mater. Manuf. Processes 2019, 34, 357–368.
7. Singh, B.P.; Singh, R.; Mehta, J.S.; Prakash, C. August. Fabrication of biodegradable low elastic porous Mg-Zn-Mn-HA alloy by spark plasma sintering for orthopaedic applications. In IOP Conference Series Materials Science and Engineering; IOP Publishing: Bristol, UK, 2017; Volume 225, p. 012050.
8. Prakash, C.; Singh, S.; Verma, K.; Sidhu, S.S.; Singh, S. Synthesis and characterization of Mg-Zn-Mn-HA composite by spark plasma sintering process for orthopedic applications. Vacuum 2018, 155, 578–584.
9. Sharma, S.K.; Kodli, B.K.; Saxena, K.K. Micro Forming and its Applications: An Overview. Key Eng. Mater. 2022, 924, 73–91.
10. Sharma, S.K.; Saxena, K.K.; Kumar, K.B.; Kumar, N. The effect of reinforcements on the mechanical properties of AZ31 composites prepared by powder metallurgy: An overview. Mater. Today Proc. 2022, 56, 2293–2299.
11. Dutta, S.; Gupta, S.; Roy, M. Recent developments in magnesium metal–matrix composites for biomedical applications: A Review. ACS Biomater. Sci. Eng. 2020, 6, 4748–4773.
12. Huynh, V.; Ngo, N.K.; Golden, T.D. Surface activation and pretreatments for biocompatible metals and alloys used in biomedical applications. Int. J. Biomater. 2019, 2019, 3806504.
13. Zheng, Y.F.; Gu, X.N.; Witte, F. Biodegradable metals. Mater. Sci. Eng. R Rep. 2014, 77, 1–34.
14. Li, Q.; Zhong, X.; Hu, J.; Kang, W. Preparation and corrosion resistance studies of zirconia coating on fluorinated AZ91D magnesium alloy. Prog. Org. Coat. 2008, 63, 222–227.

15. Rojaee, R.; Fathi, M.; Raeissi, K. Controlling the degradation rate of AZ91 magnesium alloy via sol–gel derived nanostructured hydroxyapatite coating. Mater. Sci. Eng. C 2013, 33, 3817–3825.
16. Bommala, V.K.; Krishna, M.G.; Rao, C.T. Magnesium matrix composites for biomedical applications: A review. J. Magnes. Alloy. 2019, 7, 72–79.
17. Pal, K.; Asthana, N.; Aljabali, A.A.; Bhardwaj, S.K.; Kralj, S.; Penkova, A.; Gomes de Souza, F. A critical review on multifunctional smart materials ‘nanographene’emerging avenue: Nano-imaging and biosensor applications. Crit. Rev. Solid State Mater. Sci. 2021, 5, 1–17.
18. Panda, P.; Pal, K.; Chakroborty, S. Smart advancements of key challenges in graphene-assembly glucose sensor technologies: A mini review. Mater. Lett. 2021, 303, 130508.
19. Aljabali, A.A.; Al Zoubi, M.S.; Al-Batayneh, K.M.; Pardhi, D.M.; Dua, K.; Pal, K.; Tambuwala, M.M. Innovative Applications of Plant Viruses in Drug Targeting and Molecular Imaging-A Review. Curr. Med. Imaging 2021, 17, 491–506.
20. Santhosh, S.K.; Sarojini, S.; Umesh, M. Anti-Biofilm Activities of Nanocomposites Current Scopes and Limitations. In Bio-manufactured Nanomaterials; Springer: Cham, Switzerland, 2021; pp. 83–94.
21. Jayasathyakawin, S.; Ravichandran, M.; Baskar, N.; Chairman, C.A.; Balasundaram, R. Magnesium matrix composite for biomedical applications through powder metallurgy–Review. Mater. Today Proc. 2020, 27, 736–741.
22. Kabir, H.; Munir, K.; Wen, C.; Li, Y. Recent research and progress of biodegradable zinc alloys and composites for biomedical applications: Biomechanical and biocorrosion perspectives. Bioact. Mater. 2021, 6, 836–879.
23. Hussein, M.A.; Azeem, M.A.; Kumar, A.M.; Emara, N.M. Processing and in vitro Corrosion Analysis of Sustainable and Economical Eggshell Reinforced Mg and Mg-Zr Matrix Composite for Biomedical Applications. Mater. Today Commun. 2022, 32, 103944.
24. Asiya, S.I.; Pal, K.; Kralj, S.; El-Sayyad, G.S.; de Souza, F.G.; Narayanan, T. Sustainable preparation of gold nanoparticles via green chemistry approach for biogenic applications. Mater. Today Chem. 2020, 17, 100327.
25. Singh, G.; Singh, S.; Prakash, C.; Ramakrishna, S. On investigating the soda-lime shot blasting of AZ31 alloy: Effects on surface roughness, material removal rate, corrosion resistance, and bioactivity. J. Magnes. Alloy. 2021, 9, 1272–1284.
26. Prakash, C.; Singh, S.; Ramakrishna, S. Characterization of indigenously coated biodegradable magnesium alloy primed through novel additive manufacturing assisted investment casting. Mater. Lett. 2020, 275, 128137.

27. Bauer, J.C.; Chen, X.; Liu, Q.; Phan, T.H.; Schaak, R.E. Converting nanocrystalline metals into alloys and intermetallic compounds for applications in catalysis. J. Mater. Chem. 2008, 18, 275–282.
28. Polmear, I.J. Magnesium alloys and applications. Mater. Sci. Technol. 1994, 10, 1–16.
29. Prasad, A.; Uggowitzer, P.J.; Shi, Z.; Atrens, A. Production of high purity magnesium alloys by melt purification with Zr. Adv. Eng. Mater. 2012, 14, 477–490.
30. Ouyang, L.Z.; Yang, X.S.; Zhu, M.; Liu, J.W.; Dong, H.W.; Sun, D.L.; Zou, J.; Yao, X.D. Enhanced hydrogen storage kinetics and stability by synergistic effects of in situ formed CeH2. 73 and Ni in CeH2. 73-MgH2-Ni nanocomposites. J. Phys. Chem. C 2014, 15, 7808–7820.
31. Habibnejad-Korayem, M.; Mahmudi, R.; Poole, W.J. Enhanced properties of Mg-based nano-composites reinforced with Al2O3 nano-particles. Mater. Sci. Eng. A 2009, 519, 198–203.
32. Feyerabend, F.; Fischer, J.; Holtz, J.; Witte, F.; Willumeit, R.; Drücker, H.; Vogt, C.; Hort, N. Evaluation of short-term effects of rare earth and other elements used in magnesium alloys on primary cells and cell lines. Acta Biomater. 2010, 6, 1834–1842.
33. Zhang, J.; Niu, X.; Qiu, X.; Liu, K.; Nan, C.; Tang, D.; Meng, J. Effect of yttrium-rich misch metal on the microstructures, mechanical properties and corrosion behavior of die cast AZ91 alloy. J. Alloys Compd. 2009, 471, 322–330.
34. Jafari, H.; Rahimi, F.; Sheikhsofla, Z. In vitro corrosion behavior of Mg-5Zn alloy containing low Y contents. Mater. Corros. 2016, 67, 396–405.
35. Mordike, B.L. Creep-resistant magnesium alloys. Mater. Sci. Eng. A 2002, 324, 103–112.
36. Zhang, Y.; Gore, P.; Rong, W.; Wu, Y.; Yan, Y.; Zhang, R.; Birbilis, N. Quasi-in-situ STEM-EDS insight into the role of Ag in the corrosion behaviour of Mg-Gd-Zr alloys. Corros. Sci. 2018, 136, 106–118.
37. Zhu, L.; Song, G. Improved corrosion resistance of AZ91D magnesium alloy by an aluminium-alloyed coating. Surf. Coat. Technol. 2006, 200, 2834–2840.
38. Pan, H.; Ren, Y.; Fu, H.; Zhao, H.; Wang, L.; Meng, X.; Qin, G. Recent developments in rare-earth free wrought magnesium alloys having high strength: A review. J. Alloys Compd. 2016, 663, 321–331.
39. Cao, X.J.; Jahazi, M.; Immarigeon, J.P.; Wallace, W. A review of laser welding techniques for magnesium alloys. J. Mater. Processing Technol. 2006, 171, 188–204.
40. Agarwal, S.; Curtin, J.; Duffy, B.; Jaiswal, S. Biodegradable magnesium alloys for orthopaedic applications: A review on corrosion, biocompatibility and surface modifications. Mater. Sci. Eng. C 2016, 68, 948–963.

41. Gialanella, S.; Malandruccolo, A. Alloys for aircraft structures. In Aerospace Alloys; Springer: Cham, Switzerland, 2020; pp. 41–127.
42. Sharma, S.K.; Saxena, K.K. Effects on microstructure and mechanical properties of AZ31 reinforced with CNT by powder metallurgy: An overview. Mater. Today Proc. 2022, 56, 2038–2042.
43. Sharma, S.K.; Saxena, K.K. An outlook on the influence on mechanical properties of AZ31 reinforced with graphene nanoparticles using powder metallurgy technique for biomedical application. Mater. Today Proc. 2022, 56, 2278–2287.
44. Li, L.; Li, D.; Zeng, X.; Luo, A.A.; Hu, B.; Sachdev, A.K.; Ding, W. Microstructural evolution of Mg-Al-Re alloy reinforced with alumina fibers. J. Magnes. Alloy. 2020, 8, 565–577.
45. Pettersen, G.; Westengen, H.; Høier, R.; Lohne, O. Microstructure of a pressure die cast magnesium—4wt.% aluminium alloy modified with rare earth additions. Mater. Sci. Eng. A 1996, 207, 115–120.
46. Alibabaei, S.; Kasiri-Asgarani, M.; Bakhsheshi-Rad, H. Investigating the effect of solid solution treatment on the corrosion properties of biodegradable Mg-Zn-RE-xCa (x= 0 2019, 2.5) alloy. J. Simul. Anal. Nov. Technol. Mech. Eng. 2019, 12, 67–80.
47. Yao, S.; Liu, S.; Zeng, G.; Li, X.; Lei, T.; Li, Y.; Du, Y. Effect of manganese on microstructure and corrosion behavior of the Mg-3Al alloys. Metals 2019, 9, 460.
48. Witte, F.; Feyerabend, F.; Maier, P.; Fischer, J.; Störmer, M.; Blawert, C.; Dietzel, W.; Hort, N. Biodegradable magnesium hydroxyapatite metal matrix composites. Biomaterials 2007, 28, 2163–2174.
49. Chu, A.; Zhao, Y.; Ud-Din, R.; Hu, H.; Zhi, Q.; Wang, Z. Microstructure and properties of Mg-Al-Ca-Mn alloy with high Ca/Al ratio fabricated by hot extrusion. Materials 2021, 14, 5230.
50. Rosalbino, F.; Carlini, R.; Soggia, F.; Zanicchi, G.; Scavino, G. Influence of rare earth metals addition on the corrosion behaviour of copper in alkaline environment. Corros. Sci. 2012, 58, 139–144.
51. Kiełbus, A.; Jarosz, R.; Gryc, A. Effect of modification on microstructure and properties of AZ91 magnesium alloy. Crystals 2020, 10, 536.
52. Birbilis, N.; Easton, M.A.; Sudholz, A.D.; Zhu, S.M.; Gibson, M.A. On the corrosion of binary magnesium-rare earth alloys. Corros. Sci. 2009, 51, 683–689.
53. Gu, X.N.; Xie, X.H.; Li, N.; Zheng, Y.F.; Qin, L.J.A.B. In vitro and in vivo studies on a Mg–Sr binary alloy system developed as a new kind of biodegradable metal. Acta Biomater. 2012, 8, 2360–2374.

54. Mert, F.; Blawert, C.; Kainer, K.U.; Hort, N. Influence of cerium additions on the corrosion behaviour of high pressure die cast AM50 alloy. Corros. Sci. 2012, 65, 145–151.
55. StJohn, D.H.; Easton, M.A.; Qian, M.; Taylor, J.A. Grain refinement of magnesium alloys: A review of recent research, theoretical developments, and their application. Metall. Mater. Trans. A 2013, 44, 2935–2949.
56. Manivasagam, T.G.; Kiraz, K.; Notten, P.H. Electrochemical and optical properties of magnesium-alloy hydrides reviewed. Crystals 2012, 2, 1410–1433.
57. Akbaripanah, F.; Fereshteh-Saniee, F.; Mahmudi, R.; Kim, H.K. Microstructural homogeneity, texture, tensile and shear behavior of AM60 magnesium alloy produced by extrusion and equal channel angular pressing. Mater. Des. 2013, 43, 31–39.
58. Sun, X.; Su, Y.; Huang, Y.; Chen, M.; Liu, D. Microstructure Evolution and Properties of β-TCP/Mg-Zn-Ca Biocomposite Processed by Hot Extrusion Combined with Multi-Pass ECAP. Metals 2022, 12, 685.
59. Zhang, X.; Wang, Z.; Zhou, Z.; Xu, J. Effects of cerium and lanthanum on the corrosion behavior of Al-3.0 wt.% Mg alloy. J. Mater. Eng. Perform. 2016, 25, 1122–1128.
60. Grimm, M.; Lohmüller, A.; Singer, R.F.; Virtanen, S. Influence of the microstructure on the corrosion behaviour of cast Mg-Al alloys. Corros. Sci. 2019, 155, 195–208.
61. Ünlü, B.S. Investigation of tribological and mechanical properties Al2O3–SiC reinforced Al composites manufactured by casting or P/M method. Mater. Des. 2008, 29, 2002–2008.
62. Chang, I.; Cai, Q. From simple binary to complex multicomponent eutectic alloys. Prog. Mater. Sci. 2022, 123, 100779.
63. Predko, P.; Rajnovic, D.; Grilli, M.L.; Postolnyi, B.O.; Zemcenkovs, V.; Rijkuris, G.; Pole, E.; Lisnanskis, M. Promising Methods for Corrosion Protection of Magnesium Alloys in the Case of Mg-Al, Mg-Mn-Ce and Mg-Zn-Zr: A Recent Progress Review. Metals 2021, 11, 1133.
64. Krawiec, H.; Stanek, S.; Vignal, V.; Lelito, J.; Suchy, J.S. The use of microcapillary techniques to study the corrosion resistance of AZ91 magnesium alloy at the microscale. Corros. Sci. 2011, 53, 3108–3113.